

The Structure of the Circumstellar Gas of SN 1987A

Peter Lundqvist

Stockholm Observatory, SE-133 36 Saltsjöbaden, Sweden

George Sonneborn

NASA/Goddard Space Flight Center, Code 681, Greenbelt, MD 20771

Abstract. Recent observations of the rings around SN 1987A are discussed and modeled, with particular emphasis on *HST* observations of the inner ring by the SINS¹ team. It is found that the lowest density detected in the ring is $\sim (1 - 2) \times 10^3 \text{ cm}^{-3}$. The geometry of the inner ring is constrained by its different size in [N II] and [O III]. The implications of this on the distance to the supernova are discussed and we find $\lesssim 54.2 \pm 2.2 \text{ kpc}$, which is in agreement with recent RR Lyrae and Cepheid measurements. In addition, preliminary results are presented for improved calculations of the supernova breakout.

1. Introduction

The rings of SN 1987A have been monitored by an arsenal of ground-based and space borne telescopes ever since the first detection by *IUE* of narrow circumstellar lines ~ 70 days after the explosion (Fransson et al. 1989). While the structure of the emitting gas was first displayed using *CTIO* and *Las Campanas* instruments (Crotts, Kunkel, & McCarthy 1989; Crotts, this volume) as well as the *NTT* at *ESO* (Wampler et al. 1990), the detailed structure of the rings was revealed only after the installation of *COSTAR* on *HST* (Burrows et al. 1995; Garnavich, this volume). Recently, the rings have been observed in a multitude of optical lines using *STIS* on *HST* (Pun et al. 1997), and both UV and IR studies will follow shortly.

Modeling of the emission lines during the first ~ 5 years (Lundqvist & Fransson 1996) has shown that the inner ring consists of gas with a range of densities ($\sim 6 \times 10^3 - 3 \times 10^4 \text{ cm}^{-3}$), and that it is overabundant in helium and nitrogen compared to normal LMC abundances. These models also show that emission lines can be used to constrain models of the supernova breakout. In particular, it is found that the spectrum during the breakout was probably not very different from that in the models of Ensmann & Burrows (1992), i.e., the color temperature was in the range $(1.0 - 1.5) \times 10^6 \text{ K}$. However, as is shown below, the spectrum is not a simple blackbody.

¹Supernova INTensive Study collaboration (PI: R. P. Kirshner)

Our knowledge of the physical conditions in the outer rings is more uncertain. Panagia et al. (1996) found from nebular analysis that the outer rings had an electron density of $\sim 8 \times 10^2 \text{ cm}^{-3}$, at least 2887 days after the outburst, and that the material in these rings may be less CNO-processed than in the inner ring. As argued by Crotts, Kunkel, & Heathcote (1995), and predicted by many of the models for the formation of the nebula (e.g., Blondin & Lundqvist 1993; Martin & Arnett 1995; Chevalier & Dwarkadas 1995; Chevalier, this volume), the inner and outer rings may be joined physically. It remains to be seen if this is consistent with the different mass loss episodes for the inner and outer rings, as proposed by Panagia et al. (1996).

Here we discuss and model more recent data than in Lundqvist & Fransson (1996). We focus mainly on *HST* observations until late 1996. In addition, we provide a short discussion about the distance to the supernova, and show some recent results from improved models of the supernova breakout.

2. Observations and Results

2.1. *HST* images

A detailed analysis of the structure of the inner ring was made by Plait et al. (1995) using pre-*COSTAR* images. Here we do a similar analysis for *WFPC2* images obtained 2755, 3270 and 3478 days after the outburst. While the observations themselves are discussed by Garnavich (this volume; see also Lundqvist et al. 1997b), we focus on the interpretation of the observations. In particular, we model the angle dependent fading/brightening of the ring in [N II] and [O III], since this can be used to derive the angular density distribution of the emitting gas (see Plait et al. 1995). Compared to Plait et al. (1995) our spatial resolution is significantly improved, and we include also [N II]. We emphasize that the study of Plait et al. probes gas of higher electron density ($n_e \gtrsim 8 \times 10^3 \text{ cm}^{-3}$) than our study simply because their high-density gas has now cooled and recombined, and does not contribute to the emission at our epochs. This means that we also probe gas of lower density than Lundqvist & Fransson (1996) who mainly concentrated on *IUE* data from the first ~ 1800 days.

As in Plait et al., we assume that the ring is first heated and ionized by the supernova EUV/soft X-ray burst, and then left to recombine and cool. We adopt the same model of the burst, i.e., the 500full1 model by Ensman & Burrows (1992), which was successfully used by Lundqvist & Fransson (1996) to model the light curves of the narrow UV lines observed by *IUE* (Sonneborn et al. 1997a).

We have calculated the evolution of the [N II] and [O III] emissivities for 18 densities ranging from $8.4 \times 10^2 \text{ cm}^{-3}$ to $4.2 \times 10^4 \text{ cm}^{-3}$, using equidistant steps in $\log(\text{density})$. The density we have used is the number density of atoms. The elemental abundances are H: He: C: N: O: Ne: Na: Mg: Al: Si: S: Ar: Ca: Fe = 1.0: 0.20: 4.2×10^{-5} : 1.9×10^{-4} : 1.9×10^{-4} : 6.2×10^{-5} : 1.0×10^{-6} : 1.5×10^{-5} : 1.2×10^{-6} : 1.7×10^{-5} : 5.6×10^{-6} : 3.2×10^{-6} : 1.1×10^{-6} : 3.4×10^{-5} . The abundance ratio (C+N+O)/(H+He+Z) is thus ≈ 0.35 times the solar ratio of Anders & Grevesse (1989). Note also that we assume N/O = 1. With these abundances, the electron density is ≈ 1.17 times the atomic density when the

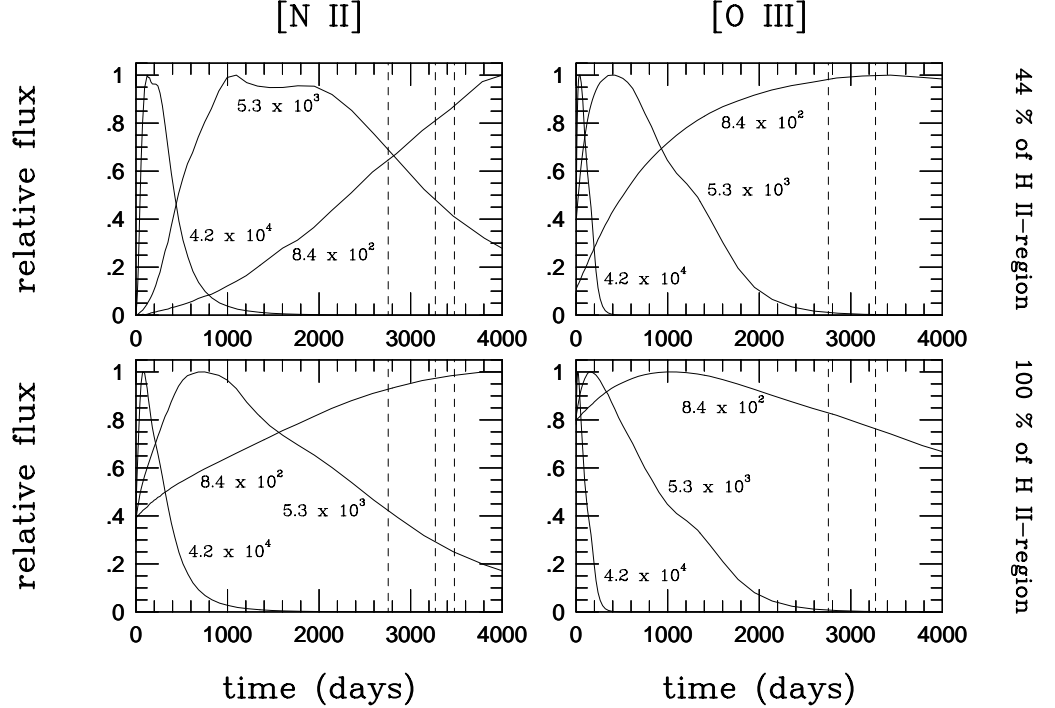


Figure 1. Evolution of relative emissivities of [N II] and [O III] from the inner ring for three single-density models: $8.4 \times 10^2 \text{ cm}^{-3}$, $5.3 \times 10^3 \text{ cm}^{-3}$ and $4.2 \times 10^4 \text{ cm}^{-3}$. The highest-density model peaks first. The bottom row of panels (100%) is for an ionization-bounded ring, while in the top row, only the 44% innermost region of the H II-region is included. (Such models are referred to as “truncated” in the text.) The observed epochs are marked with dashed vertical lines. No compensation for light travel times have been included in the figure.

gas is fully ionized. Abundances and atomic data are discussed in greater detail in Lundqvist et al. (1997a). (See also §2.2)

Figure 1 displays the evolution of the normalized emissivities of [N II] and [O III] for three of the densities. With increasing density the emissivity peaks at earlier times, $t_{\text{peak}} \propto n^{-1}$. The results shown in Figure 1 are for two cases: one is for an ionization-bounded ring of constant density, and the other (henceforth referred to as “truncated” or “density-bounded”) takes into account only the innermost 44 % of the H II-region in the ionization-bounded model. A truncated model does not necessarily have to be devoid of gas outside the cut, it may just have a sharp density drop like in the interacting-winds model (cf. Luo 1991 and Blondin & Lundqvist 1993).

Figure 1 shows that truncation affects strongly the evolution of the emissivity from the ring. For example, the maximum [N II] emission can in the ionization-bounded case only be a factor of ~ 2.5 higher than immediately after the outburst, whereas in the truncated case, arbitrarily large ratios are possible. This is because the [N II] emission in the truncated case relies on recombination from N^{2+} and higher states, while in the ionization-bounded case, N^+ is present from the outset. A similar effect is seen for [O III], though some O^{2+} is present inside the 44 %-boundary also from the outset (cf. Fig. 1 of Lundqvist & Fransson 1996). In Figure 1, we have marked our observed epochs by vertical dashed lines. (Note that for [O III] there are only two epochs included.)

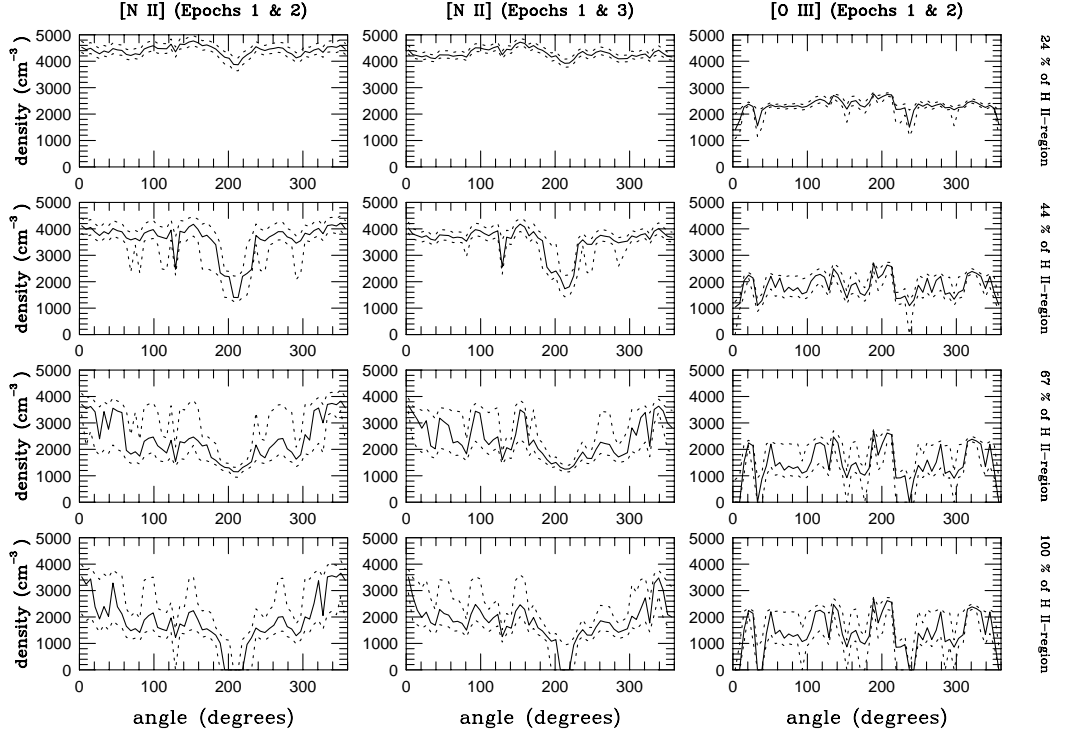


Figure 2. Modeled mean density of the inner ring as a function of position angle for four degrees of truncation of the ring. The bottom row of panels is for an ionization-bounded ring, while going upwards, the ring has been truncated closer and closer to its inner edge. Solid lines are for the measured ratios of fluxes between the epochs listed at the top of each column, whereas dotted lines are for a 5% uncertainty of these ratios. Light travel times have been included.

To compare Figure 1 with the observed position-angle (PA) dependent fading/brightening between epochs, light travel times have to be included (e.g., Dwek & Felten 1992). We have assumed a tilt angle of the ring of 43 degrees and a ring radius of 6.3×10^{17} cm (e.g., Sonneborn et al. 1997a). This gives minimum and maximum shifts between the observed epoch and the epoch of emission of ~ 77 days (for PA ~ 0 degrees) and ~ 409 days (for PA ~ 180 degrees), respectively. As these numbers are much smaller than the number of days since the explosion at the observed epochs, correction for light travel times is less important in the current study than in Plait et al. (1995).

The density corresponding to the fading/rebrightening of [N II] and [O III] between the observed epochs described in Lundqvist et al. (1997b) is shown in Figure 2, where we have also added results for two other locations of the truncation (24% and 67%). The solid lines in Figure 2 correspond to the observed ratios, whereas the dotted lines correspond to a $\pm 5\%$ uncertainty of these ratios. In our analysis there are also systematic errors due to uncertainties in atomic data as well as approximations in the photoionization code. However, we believe that the dominant uncertainty affecting the estimated density is the degree of truncation. It should be emphasized that our analysis, like the one of Plait et al. (1995), only gives a mean density for each position angle. In reality, this is an average of both higher and lower values.

Figure 2 shows that the estimated density is lower in ionization-bounded models ($\sim 2 \times 10^3$ cm $^{-3}$ for [N II] and $(1 - 2) \times 10^3$ cm $^{-3}$ for [O III]) than in

truncated, especially in the case of [N II]. This is not surprising since truncated models rely on recombination to emit the optical lines. The time scale for this is $t_{\text{rec}} \propto n_e^{-1}$. Because the highest degree of ionization at the outset occurs close to the inner edge of the ring, higher densities are needed to reach N^+ at the observed epoch the more the ring is truncated. We cannot determine from Figure 2 alone the degree of truncation, though *it seems evident that at least some truncation is necessary at PA 200–210 degrees to explain the rebrightening of [N II] at that position angle* reported by Garnavich & Kirshner (1996); it is only in truncated models that one gets a sufficient increase in emissivity between the observed epochs. *The fact that truncated models are able to explain the rebrightening of [N II] also means that no additional ionizing source is needed*, which is fully consistent with the finding of Lundqvist et al. (1997a) that the observed X-ray emission (Hasinger, Aschenbach, & Trümper 1996; Hasinger, this volume) is too weak to reionize the ring. We emphasize that if the ring is truncated also at other position angles, the degree of truncation may vary around the ring. Different panels of Figure 2 may therefore apply at different position angles of the ring. We will, however, in the following assume that the same truncation applies at all position angles. We have also disregarded the effect that different position angles sample different path lengths through the ring along the line of sight. This is a simplification since observations at different position angles may bias slightly different physical conditions.

2.2. *HST* spectra

Spectra of the inner ring have been taken within the SINS collaboration at the four epochs 1864, 2228, 2876 and 3262 days. (Each of these epochs is actually a “mean epoch” weighted by exposure time.) A full description and analysis of the spectra is done in Lundqvist et al. (1997a), and a nebular analysis is provided by Panagia, Scuderi, & Gilmozzi (this volume). Most of the lines identified by Lundqvist et al. were identified prior to the *HST* observations (Wang 1991; Cumming 1994; Sonneborn et al. 1997a), but many are reported here, and by Lundqvist et al. (1997a), for the first time, especially lines in the UV due to the higher sensitivity of the *HST* compared to the *IUE*. Previously unidentified lines are: He I $\lambda 3188$, He I $\lambda 4388$, He II $\lambda 2734$, He II $\lambda 3203$, C II] $\lambda 2326$, [N I] $\lambda \lambda 5198, 5200$, [N II] $\lambda \lambda 2139, 2143$, [N II] $\lambda 3063$, [O II] $\lambda 2470$, [Ne IV] $\lambda \lambda 2422, 2424$, [Ne V] $\lambda 2975$, [Ne V] $\lambda \lambda 3346, 3426$, Mg I] $\lambda 4792$, Si III $\lambda \lambda 1883, 1892$, [Fe II] $\lambda \lambda 4287, 4416$ and [Fe III] $\lambda 4702$. As an example of the spectra, we show in Figure 3 selected parts of the day 2876 spectrum. This observation was centered on the brightest part of the ring, i.e., that at PA 300 degrees.

The dominant lines at all four epochs are [N II] $\lambda \lambda 6548, 6583$. Combined with [N II] $\lambda 5755$, these give a temperature of $\sim 1.0 \times 10^4$ K at all epochs. (We have assumed $E(B - V) = 0.16$, in accordance with Sonneborn et al., 1997a). The temperature derived from the [N II] UV doublet, $I_{\lambda \lambda 2139, 2143} / I_{\lambda 5755}$ is 30 – 50% higher. This is accounted for by the fact that the UV doublet has a higher excitation energy than [N II] $\lambda \lambda 6548, 6583$, which means that the UV doublet is primarily emitted in regions with higher temperature than those emitting the [N II] $\lambda \lambda 6548, 6583$ lines. The temperature derived from [O III] $\lambda \lambda 4959, 5007$ and [O III] $\lambda 4363$ is even higher, $(2.3 - 3.0) \times 10^4$ K.

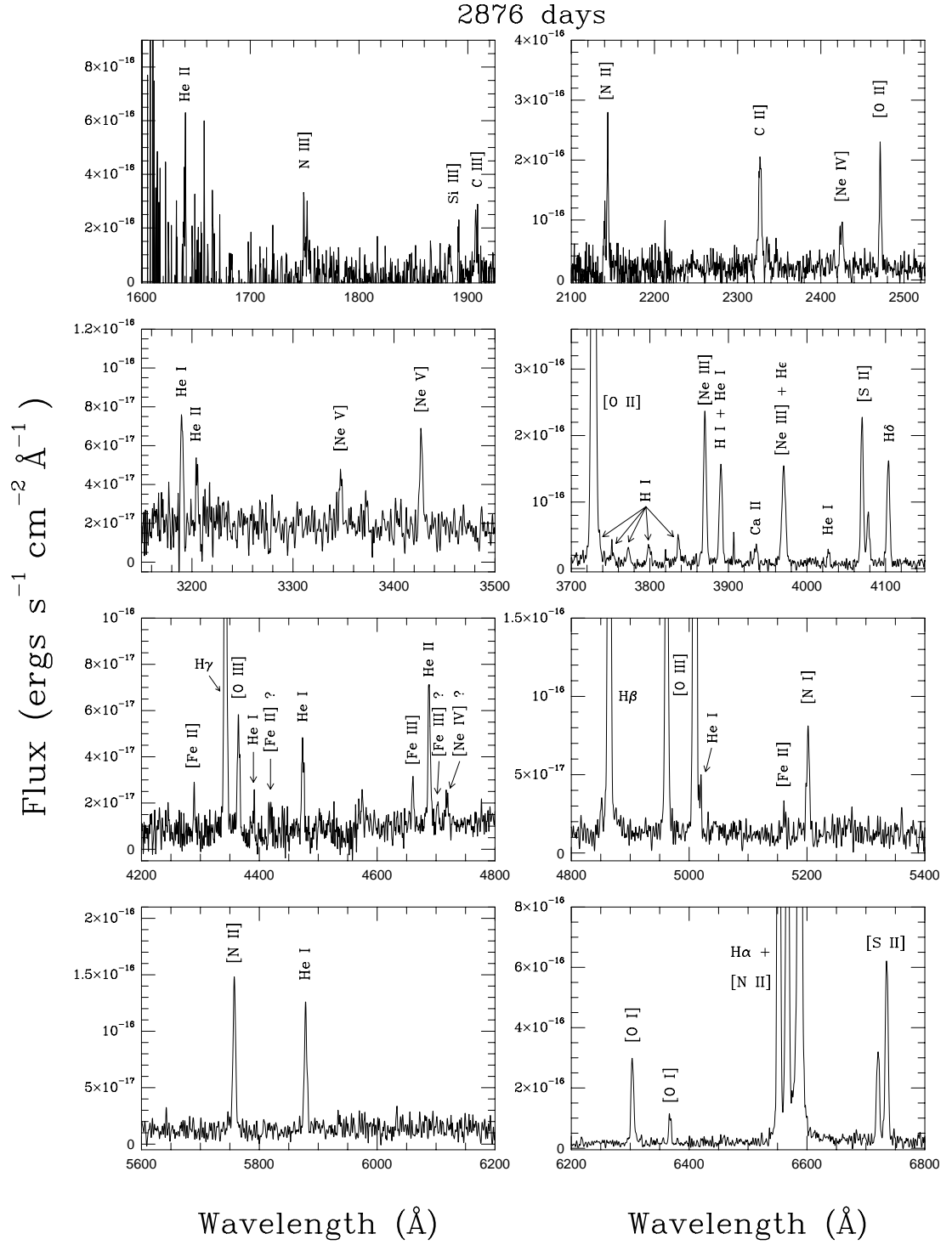


Figure 3. *HST/FOS* spectrum of the inner ring at PA 300 degrees at 2876 days. Both clear and tentative line identifications have been marked. The spectrum has not been dereddened.

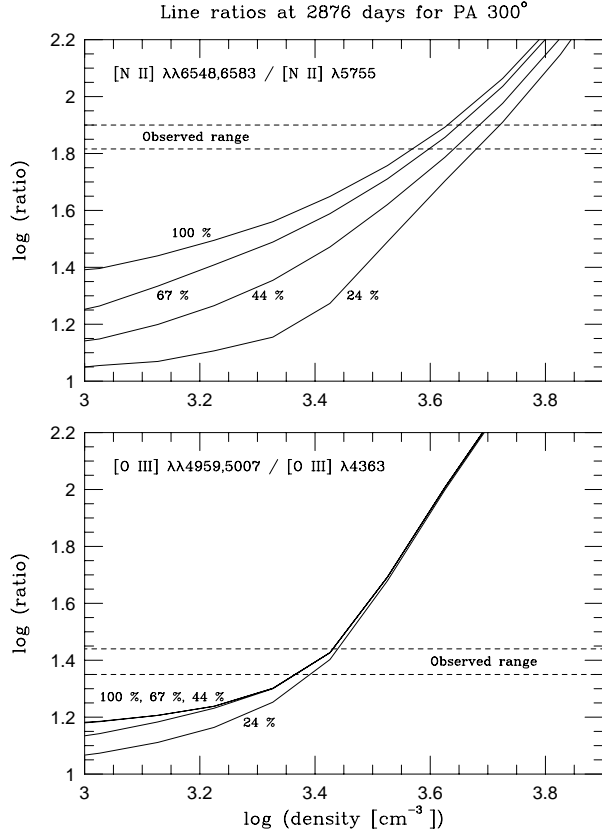


Figure 4. [N II] and [O III] line ratios for PA 300 degrees at 2876 days as functions of density for the four degrees of truncation described in the text (solid lines). Dashed lines show the observed range of the *HST/FOS* observations of Lundqvist et al. (1997a) at the same epoch. Note that the [N II] density is a factor of ~ 2 higher than that of [O III], and that neither of these densities are as sensitive to truncation as the densities in Figure 2.

Densities are most easily obtained from [O II] and [S II] line ratios. In general, the [S II] $\lambda\lambda 6716, 6731$ lines yield $\sim 1.0 \times 10^4 \text{ cm}^{-3}$, whereas the more highly excited [S II] $\lambda\lambda 4069, 4076$ lines give a somewhat lower density, and indicate a [S II] temperature of $\lesssim 10^4 \text{ K}$ after ~ 2228 days. The [O II] densities are lower ($\text{few} \times 10^3 \text{ cm}^{-3}$) and indicate temperatures approaching $2 \times 10^4 \text{ K}$.

The abundances estimated from modeling of the spectra (Lundqvist et al. 1997a) are close to those listed in §2.1. Apart from the elements discussed in detail by Lundqvist & Fransson (1996), neon appears to be consistent with its normal LMC abundance, while silicon is underabundant by a factor of ~ 2 . The low silicon abundance could be due to depletion caused by grain formation in the red supergiant wind of the progenitor prior to the explosion. An argument along the same line was put forward by Borkowski, Blondin, & McCray (1997) for a low iron abundance. Unfortunately, the iron lines detected by *HST* are too weak, and atomic data for iron is rather poor, so we cannot confirm their low iron abundance. However, an analysis of ground-based data from *ESO/NTT* is underway (Cumming & Lundqvist, in preparation).

3. Discussion

3.1. Consistency check of density from spectra and images

To distinguish between the densities in Figure 2, and thus the importance of truncation, we have compared our findings in §2.1 to the densities derived by Lundqvist et al. (1997a). We concentrate on their observation at 2876 days (see Fig. 3) since this is the closest in time to the epochs of the images. Just as for 2876 days, the spectrum at 3262 days was taken of the brightest part of the ring. For both epochs Lundqvist et al. derive [N II] and [O III] temperatures of $\sim 1.0 \times 10^4$ K, and $\sim 2.7 \times 10^4$ K, respectively. In Figure 4, we compare their dereddened intensity ratios for [N II], $I_{\lambda\lambda 6548,6583}/I_{\lambda 5755}$, and for [O III], $I_{\lambda\lambda 4959,5007}/I_{\lambda 4363}$, with ratios obtained from the truncated and ionization-bounded single-density models discussed in Figures 1 and 2. For the observed ratios we have assumed an uncertainty of $\pm 10\%$.

Figure 4 shows that the ratio of the [O III] lines favors a mean density of $(2.5 \pm 0.3) \times 10^3 \text{ cm}^{-3}$, rather independent on the amount of truncation. This is consistent with the [O III] density at PA 300 degrees in Figure 2, especially in the case of the 24%-model. Because we cannot expect a mean density found from the fading of the [O III] $\lambda 5007$ emission to be exactly the same as that found from the $I_{\lambda\lambda 4959,5007}/I_{\lambda 4363}$ ratio, none of the other models in Figure 2 can, however, be excluded by the [O III] lines. The situation is clearer for the [N II] lines. Here the temperature sensitive ratio gives a density of $(5.0 \pm 0.3) \times 10^3 \text{ cm}^{-3}$ for the 24%-model, decreasing down to $(4.0 \pm 0.3) \times 10^3 \text{ cm}^{-3}$ for the ionization-bounded model. Comparing with the first column of panels in Figure 4, which corresponds best in time to the *FOS* observations, best agreement is again obtained for the 24%-model, while both the 67% and ionization-bounded models can probably be excluded. Assuming that the degree of truncation be the same around the ring, Figures 2 and 4 show that the average density of the [N II]-emitting gas is probably in excess of $\sim 4.0 \times 10^3 \text{ cm}^{-3}$, while that of the [O III]-emitting gas is $\sim (2.0 - 2.5) \times 10^3 \text{ cm}^{-3}$.

The slightly higher density we find for [N II] than [O III] is in accordance with the fact that [S II] $\lambda\lambda 6716, 6731$ comes from gas of even higher density; at 2876 days Lundqvist et al. (1997a) find that the [S II] density is $\sim 9 \times 10^3 \text{ cm}^{-3}$. On the other hand, a density derived from [O II] $\lambda\lambda 3726, 3729$ should be lower than that characterizing the [N II] emission, despite the same ionization stage. This is because the [O II] lines have higher excitation energies, and are therefore biased towards hotter gas, i.e., low-density gas that has not cooled down to 10^4 K. Lundqvist et al. (1997a) find a density from [O II] which is similar to ours for the [O III] lines, as well as that estimated by Panagia et al. (1996) from [O II] $\lambda\lambda 3726, 3729$ at 2887 days.

Because our images show a bias for the [N II] emission towards the inner edge of the [O III] ring, we speculate that the [S II] emission should spatially trace the [N II] emission, while the [O II] $\lambda\lambda 3726, 3729$ emission probably correlates more with the [O III] emission. The [O II] $\lambda\lambda 7320-7330$ multiplet, however, could be more concentrated to the [N II] emission, since it has a lower excitation energy than [O II] $\lambda\lambda 3726, 3729$. Emission in [O I] $\lambda\lambda 6300, 6364$ may trace even higher densities than [S II]. Observations using *STIS* should soon sort this out.

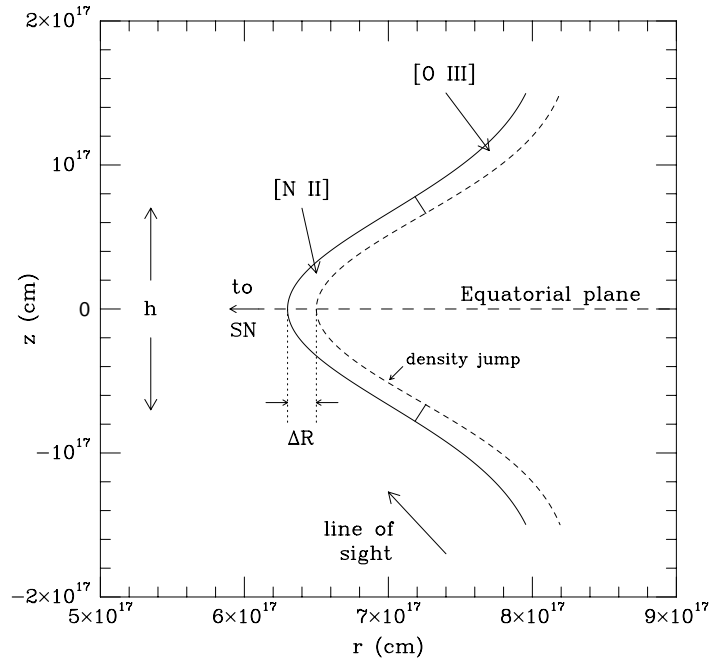


Figure 5. Sketched cross section of the ring in its equatorial plane. The figure is only intended to show the rough properties of the ring rather than its exact geometry. As indicated by the arrow showing the line of sight, the cross section applies to PA 0 degrees. The [N II] emission comes from close to the equatorial plane, whereas [O III] comes from regions more distant from the supernova, as well as further from the equatorial plane. The boundary between these regions is indicated by a solid line, though there is most likely a more gradual decline in density with increasing $|z|$. The figure only shows the structure for $|z| < 1.5 \times 10^{17}$ cm since there is no information from the HST images how the ring connects to the outer rings of the supernova. The label “density jump” refers to the fact that the [N II]-emitting gas appears to be density-bounded rather than ionization-bounded. The high-density gas observed by *IUE* ($n_e \sim \text{few} \times 10^4 \text{ cm}^{-3}$) is probably correlated with the [N II] region in the figure. The parameters ΔR and h are described in the text.

3.2. Geometry of the inner ring

We now discuss a viable geometrical model to explain the observed structure of the emitting gas in the inner ring. In particular, the model must explain why the observed [N II] emission comes from a region inside the [O III] region, and why it is thinner (Garnavich, this volume; §3.3 below). Because we have found that $n_{[\text{N II}]} > n_{[\text{O III}]}$ this means that low-density gas is situated, on average, outside that of higher density. From the analysis in Lundqvist et al. (1997a), the most consistent explanation is that R_{in} , the inner radius of the observed ring, is different for the emission in [N II] and [O III]. If this is correct, it is natural to assume that there is a continuous change in density from the [N II] region to the [O III] region, and that the two regions are joined physically. It is also important that we explain why the observed thickness of the [N II] gas appears to be roughly the same at the ring’s semiminor and semimajor axes. This cannot be done with a ring which has $h \gg \Delta R_{[\text{N II}]}$ (where h is the total extent of the ring perpendicular to the intrinsic plane of the ring and $\Delta R_{[\text{N II}]}$ the

radial thickness of the [N II] ring in the same plane), unless the inner surface of the ring has a radius which changes significantly with distance above and below the plane of the ring.

The situation envisaged is thus similar to the ionized-on-the-inside-only crescent discussed in Plait et al. (1995), only that in our case we do not argue for ionization marking the boundary between emitting and non-emitting gas. In our model the nebula observed by *HST* after ~ 2755 days is density-bounded.

Figure 5 shows a cross section of the ring in this model. The particular part of the ring we have chosen to show is at PA 0 degrees. The model is the same for other position angles, only that the line of sight will be different. Due to the brightness variation with position angle, it is obvious that the ring is not axisymmetric, so Figure 5 is only meant to be a rough representation of the real ring. In particular, ΔR , h and R_{in} are all likely to vary with position angle. In addition, we do not know the exact curvature of the ring as a function of z , i.e., the distance perpendicular to the plane of the ring. However, because of the rather well-determined tilt angle of the ring, the curvature cannot be very different from that in Figure 5 to obtain [N II] on the inside of the [O III] emission in the observed image.

Another benefit from our model is that it can account for the fact that both the [N II] and [O III] emission extends over a large radius, ΔR_{obs} , corresponding to $\Delta R_{\text{obs}}/R_{\text{in}} \sim 0.1 - 0.2$, and that it does so for all position angles. For a ring with no curvature with increasing $|z|$, this cannot be the case for PA 90 and 270 degrees, especially if the ring has a filling factor close to unity. With the model in Figure 5 there is no need for a low filling factor in the *emitting* region; it is only in *projection* the filling factor is low for a given line of sight.

Our model predicts that the [N II] emission will eventually venture into the region now emitting [O III], thus increasing in observed size. At the same time, the high-density gas closest to the supernova will cool and fade in [N II]. The [O III] nebula may also increase in size if there are regions of lower density outside the present nebula.

It is interesting that our geometrical model (Fig. 5) bears resemblance with the *structure* close to the equatorial plane in the models of Blondin & Lundqvist (1993) and Martin & Arnett (1995). In both simulations, the structure curves out toward larger r with increasing $|z|$. Ground-based (e.g., Crotts, this volume) and deeper *HST* images are needed to compare modeled and observed structures at large z . However, as noted by Lundqvist & Fransson (1996), we already know that neither the models of Blondin & Lundqvist nor those of Martin & Arnett are likely to adequately model the structure as far above and below the equatorial plane as the outer rings.

Our constraints on the geometry and density of the ring are important also for the modeling of the forthcoming ejecta/ring interaction (Borkowski et al. 1997). The most obvious change to the model of Borkowski et al. is that there will be no shock entering the ring from “behind”, i.e., the side of the ring opposite to that facing the supernova, unless the ring is broken up in the third dimension. With the relative distribution of components with different densities discussed in Lundqvist et al. (1997a,b), better predictions of the line emission from the ejecta/ring nebula can be made. Conversely, our model of the nebula

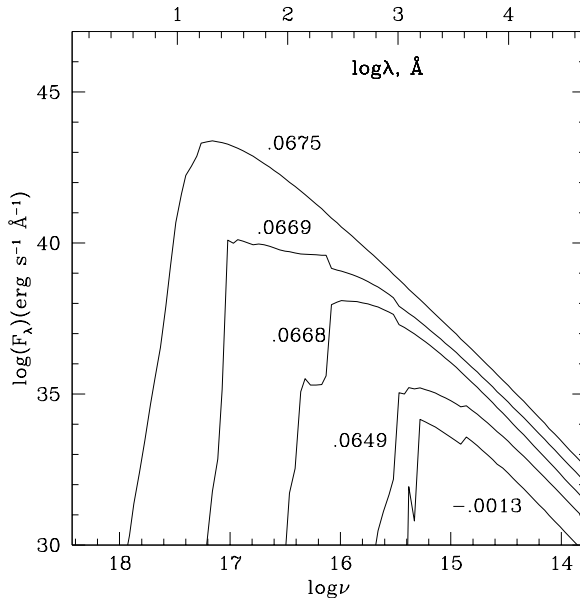


Figure 6. Spectral flux in observer's frame at shock breakout. The progenitor model has a mixed composition and is from Saio, Nomoto, & Kato (1988) and Shigeyama, Nomoto, & Hashimoto (1988). The mass of the star is $16.3 M_{\odot}$ and its radius is 3.4×10^{12} cm. The mass cut is at $1.6 M_{\odot}$ and the explosion energy is 1.3×10^{51} ergs. The curves are labeled by retarded time in days.

can be tested as the ejecta start interacting with different parts of the ring at different times.

3.3. Distance to the supernova

Panagia et al. (1991) devised a simple way to estimate the distance to SN 1987A using the *IUE* light curves of the narrow lines, in combination with *HST* imaging observations. The method assumes a perfect match between the geometry of the UV-line emitting gas around day 80 to 400 and that emitting [O III] \sim 1000 days later. It is also thought that the gas does not have to recombine before emitting the UV-lines, and the ring is assumed to be intrinsically circular. Later, Gould (1995) used a similar approach including a more sophisticated statistical treatment. Both studies argued for rather small errors, but did not agree on the inferred distance (51.2 ± 3.1 kpc and $\lesssim 46.77 \pm 0.76$ kpc, respectively). Recently, both groups have reevaluated their distances (Panagia, Gilmozzi, & Kirshner, this volume; Gould & Uza 1997, preprint) now obtaining 51.5 ± 1.2 kpc and $\lesssim 48.76 \pm 1.13$ kpc, respectively, still inconsistent with each other. Using the same method Sonneborn et al. (1997a) obtained 48.6 ± 2.2 kpc, assuming the [O III] angular diameter of Plait et al. (1995).

It is obvious that the real error of these estimates could be arbitrarily large simply because the gas once dominating the UV-line emission has a high density and faded before the first *HST* images were taken. To minimize the error one should measure the angular size of the ring in lines tracing the same gas as that emitting the UV lines during the first ~ 400 days. Obviously, [N II], and especially [O III], are not ideal in that sense, at least not at present epochs. Instead, one should observe lines emitted by ions that have recombined further.

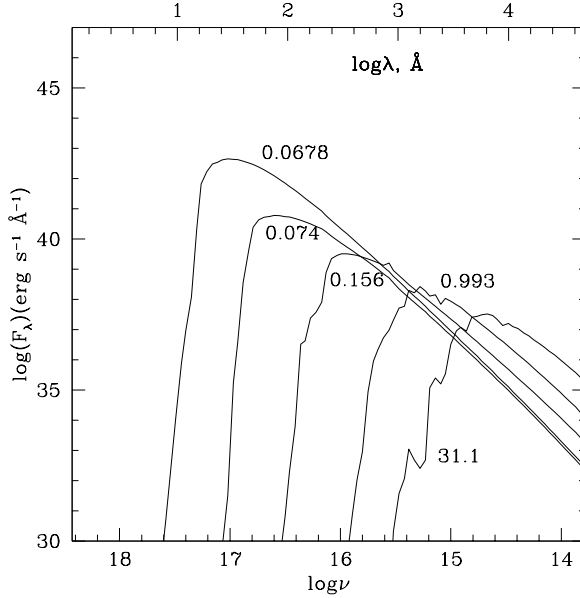


Figure 7. Same as Fig. 6, but after shock breakout.

Both [S II] and [O I] should be better, though [S II] may only be marginally better than the [O III] observations of Plait et al. (1995), which indicated emission from gas of the same density as [S II] indicates today. [O I] observations have now been made using *STIS* (Pun et al. 1997; Sonneborn et al. 1997b), and we will include this line in future analyses.

Meanwhile, our geometrical model in Figure 5, together with the models of Lundqvist & Fransson (1996), suggest that the innermost region of the [N II] region is likely to give a reasonable estimate of where the first UV emission lines came from. The time of turn on of the UV lines, t_{\min} , is therefore related to R_{in} of [N II], while the time when the UV lines peak, t_{\max} , depends on how far from the equatorial plane the high-density gas reaches, as well as the off-equatorial geometry of the ring. The most conservative assumption is that t_{\max} corresponds to a radius which is $\gtrsim R_{\text{in}}$ of [N II]. From the *HST* images in §2.1 we find that the angular extent corresponding to R_{in} of [N II] could be as low as $\sim 770 \pm 20$ mas. We combine this with $t_{\min} = 84 \pm 4$ days and $t_{\max} = 399 \pm 15$ days from Sonneborn et al. (1997a), and obtain a distance to the supernova which is $\lesssim 54.2 \pm 2.2$ kpc. While this is only an upper limit, it is consistent with recent estimates of RR-Lyraes and Cepheids (Reid 1997; Gratton et al. 1997; Feast & Catchpole 1997), which all indicate values around our limit. We emphasize that a model assuming an infinitesimally thin ring combined with published mean values of the angular extent of the ring can give unreliable estimates.

3.4. What is next?

Future progress in our knowledge about the rings, and the circumstellar nebula in general, relies on continued monitoring, especially with *HST*, as well as more refined modeling. The most problematic point on the modeling side is that there is no convincing model for the formation of the outer rings. Hopefully

this meeting has sparked some new ideas about that. The model of Chevalier & Dwarkadas (1995; see also Chevalier, this volume) appears to be on the right track, and maybe we can learn something from the rings around the star Sher #25 and other blue stars with rings (Chu, Brandner, & Grebel, this volume).

More detailed analysis of the emission lines from the rings requires more detailed calculations of the ionizing spectrum at shock breakout. Such calculations are in progress using a multigroup method and accurate expansion opacities (Blinnikov et al. 1997; see also Nomoto, Blinnikov, & Iwamoto, this volume). An example of these calculations is shown in Figures 6 and 7, where also the parameters of the model are given. Although the effective temperature is close to that in the models of Ensman & Burrows (1992), the spectrum is different from a superposition of blackbody spectra.

Finally, progress in our understanding of the rings also requires ground-based observations to pick up weak lines necessary for accurate abundance analyses, as well as to determine the velocity field (e.g., Crotts, this volume).

Acknowledgments. We are grateful to the SINS team for collaboration. P.L. wishes to thank Oleg Bartunov, Sergei Blinnikov, Peter Challis, Robert Cumming, Peter Garnavich and Garrelt Mellema for collaboration and discussions. This research was supported by the Swedish Natural Science Research Council, the Swedish National Space Board and the Wenner-Gren Center Foundation for Scientific Research.

References

- Anders, E., & Grevesse, N. 1989, *Geochimica et Cosmochimica Acta*, 53, 197
 Borkowski, K. J., Blondin, J. M., & McCray, R. 1997, *ApJ*, 476, L31
 Blinnikov, S. I., Bartunov, O. S., Lundqvist, P., Utrobin, V. P., & Nomoto, K., in preparation
 Blondin, J. M., & Lundqvist, P. 1993, *ApJ*, 405, 337
 Burrows, C. J., et al. 1995, *ApJ*, 452, 680
 Chevalier, R. A., & Dwarkadas, V. V. 1995, *ApJ*, 452, L45
 Crotts, A. P. S., Kunkel, W. E., & Heathcote, S. R. 1995, *ApJ*, 438, 724
 Crotts, A. P. S., Kunkel, W. E., & McCarthy, P. J. 1989, *ApJ*, 347, L61
 Cumming, R. J. 1994, Ph.D. thesis, Imperial College, London
 Dwek, E., & Felten, J. 1992, *ApJ*, 387, 551
 Ensman, L., & Burrows, A. 1992, *ApJ*, 393, 742
 Feast, M. W. & Catchpole, R. M. 1997, *MNRAS*, 286, L1
 Fransson, C., Cassatella, A., Gilmozzi, R., Kirshner, R. P., Panagia, N., Sonneborn, G., & Wamsteker, W. 1989, *ApJ*, 336, 429
 Garnavich, P. G., & Kirshner, R. P. 1996, *IAU Circ.*, No. 6368
 Gould, A. 1995, *ApJ*, 452, 189
 Gratton, R. G., Fusi Pecci, F., Carretta, E., Clementini, G., Corsi, C. E., & Lattanzi, M. 1997, *ApJ*, submitted

- Hasinger, G., Aschenbach, B., & Trümper, J. 1996, *A&A*, 312, L9
- Lundqvist, P., Challis, P. M., & SINS team 1997a, in preparation
- Lundqvist, P., & Fransson, C. 1996, *ApJ*, 464, 924
- Lundqvist, P., Garnavich, P. G., & SINS team 1997b, in preparation
- Luo, D. 1991, Ph.D. thesis, Univ. Colorado
- Martin, C. M., & Arnett, D. A. 1995, *ApJ*, 447, 378
- Panagia, N., Gilmozzi, R., Macchetto, F., Adorf, H.-M., & Kirshner, R. P. 1991, *ApJ*, 380, L23
- Panagia, N., Scuderi, Gilmozzi, R., Challis, P. M., Garnavich, P. G., & Kirshner, R. P. 1996, *ApJ*, 459, L17
- Plait, P. C., Lundqvist, P., Chevalier, R. A., & Kirshner, R. P. 1995, *ApJ*, 439, 730
- Pun, C. S. J., Sonneborn, G., Bowers, C., Gull, T., Heap, S., Kimble, R., Maran, S., & Woodgate, B. 1997, *IAU Circ.*, No. 6665
- Reid, I. N. 1997, *AJ*, in press
- Saio, H., Nomoto, K., & Kato 1988 *ApJ*, 331, 388
- Shigeyama, T., Nomoto, K., & Hashimoto, M. 1988, *A&A*, 196, 141
- Sonneborn, G., Fransson, C., Lundqvist, P., Cassatella, A., Gilmozzi, R., Kirshner, R. P., Panagia, N., & Wamsteker, W. 1997a, *ApJ*, 477, 848
- Sonneborn, G., et al. 1997b, *ApJ*, submitted
- Wampler, E. J., Wang, L., Baade, D., Banse, K., D’Odorico, S., Gouiffes, C., & Tarenghi, M. 1990, *ApJ*, 362, L13
- Wang, L. 1991, *A&A*, 246, L69